Identification of the endodermal vacuole as the iron storage compartment in the Arabidopsis embryo.

Hannetz Roschzttardtz, Geneviève Conéjéro, Catherine Curie, Stéphane Mari

Identification of the Endodermal Vacuole as the Iron Storage Compartment in the Arabidopsis Embryo[1]

Hannetz Roschzttardtz, Geneviève Conéjéro, Catherine Curie, and Stéphane Mari*

Laboratoire de Biochimie et Physiologie Moléculaire des Plantes, Institut de Biologie Intégrative des Plantes, Centre National de la Recherche Scientifique (UMR 5004), Institut National de la Recherche Agronomique, Université Montpellier II, Ecole Nationale Supérieure d'Agronomie, F–34060 Montpellier cedex 2, France

Deciphering how cellular iron (Fe) pools are formed, where they are localized, and which ones are remobilized represents an important challenge to better understand Fe homeostasis. The recent development of imaging techniques, adapted to plants, has helped gain insight into these events. We have analyzed the localization of Fe during embryo development in Arabidopsis (*Arabidopsis thaliana*) with an improved histochemical staining based on Perls coloration intensified by a second reaction with diaminobenzidine and hydrogen peroxide. The procedure, quick to set up and specific for Fe, was applied directly on histological sections, which dramatically increased its subcellular resolution. We have thus unambiguously shown that in dry seeds Fe is primarily stored in the endodermis cell layer, within the vacuoles, from which it is remobilized during germination. In the *vit1-1* mutant, in which the Fe pattern is disturbed, Fe is stored in vacuoles of cortex cells of the hypocotyl/radicle axis and in a single subepidermal cell layer in the cotyledons. During the early stages of embryo development, Fe is evenly distributed in the cells of both wild-type and *vit1-1* mutants. Fe eventually accumulates in endodermal cells as the vascular system develops, a process that is impaired in *vit1-1*. Our results have uncovered a new role for the endodermis in Fe storage in the embryo and have established that the Perls/diaminobenzidine staining is a method of choice to detect Fe in plant tissues and cells.

Iron (Fe) is an essential metal ion for all living organisms since it plays a pivotal function in electron transport processes. In plants, Fe is particularly crucial since it is not only important for respiration or cell division but also for the synthesis of chlorophyll and in electron transport chain of the photosynthesis. Although the capacity to accept or donate an electron is central in these processes, the reaction of ferrous Fe with oxygen can lead to the production of reactive oxygen species that are potentially toxic for the cell. Plants, as sessile organisms facing changing conditions, have developed a strict control of Fe homeostasis to cope with the duality of this element. At the whole-plant level, this mechanism relies on the regulation and integration of several functions such as root absorption, loading of the vascular system for the long-distance transport, storage, and remobilization from senescing organs. At the molecular level, several key actors of these mechanisms have been identified. The high-affinity Fe acquisition in roots is controlled by a ferric chelate reductase encoded by *AtFRO2* and a Fe^{2+} transporter encoded by *AtIRT1* (Eide et al., 1996; Robinson et al., 1999; Vert et al., 2002).

Once in root cells, Fe has to be transported toward the central cylinder to eventually enter the xylem stream. Fe loading in the xylem vessels seems to be controlled, at least in part, by the loading of citrate, which is the ligand of Fe in the xylem sap. This transport activity is apparently catalyzed by FRD3, a protein belonging to the multidrug and toxin efflux family (Green and Rogers, 2004; Durrett et al., 2007). Finally, distribution of Fe within the plant is regulated in part by the production of nicotianamine, a wide-range metal chelator, and by nicotianamine-metal transporters belonging to the Yellow Stripe1-Like family (Curie et al., 2009).

Fe distribution between tissues and within the cell has been poorly documented so far. The importance of apoplastic Fe pools has been studied mainly by biochemical approaches on roots, based on the reduction and chelation of Fe (Bienfait et al., 1985). This technique was useful to show that the root apoplast has a very high Fe-binding (and exchanging) capacity that reaches up to 1,000 μg/g of root dry weight, but does not exceed 50 μg/g in standard growth conditions (Strasser et al., 1999). The precise concentration and role of apoplastic Fe pools are still quite elusive. Within leaf cells, the chloroplast is a candidate organelle of choice for containing significant amounts of Fe because of the numerous Fe proteins present in the photosynthetic electron transfer chain. On the basis of metal measurements in subcellular fractions of Arabi-

[1] This work was supported by the Centre National de la Recherche Scientifique, l'Institut National de la Recherche Agronomique. The work of H.R. is supported by a postdoctoral fellowship from the Agence Nationale pour la Recherche (program 07–3–18–8–87 DISTRIMET).

* Corresponding author; e-mail mari@supagro.inra.fr.

The author responsible for distribution of materials integral to the findings presented in this article in accordance with the policy described in the Instructions for Authors (www.plantphysiol.org) is: Stéphane Mari (mari@supagro.inra.fr).

www.plantphysiol.org/cgi/doi/10.1104/pp.109.144444

dopsis (*Arabidopsis thaliana*) leaves, it was proposed that approximately 70% of the total Fe was located in chloroplasts, among which one-half was found in the thylakoids (Shikanai et al., 2003). As shown in mammalian cells, ferritins have been proposed to function as the main Fe store in plastids. Recently, a loss-of-function approach has shown that the importance of ferritins as the major Fe pool has been overestimated and that these proteins are rather involved in protection against oxidative damage in conditions of Fe excess (Ravet et al., 2009). Information on the establishment, localization, and mobilization of Fe pools in plant cells is thus very scarce.

In the last years, the development of imaging techniques has been crucial to obtain new insights in the location of Fe, particularly in the seeds. Energy-dispersive x-ray (EDX) microanalysis and inelastic scattered electron microscopy have been used to quantify and localize metals within cellular compartments on Arabidopsis seeds during germination. In particular, this approach has revealed that (1) globoid structures located within vacuoles contain high concentrations of Fe, (2) during germination Fe is remobilized from these globoids and, more importantly, (3) this process is blocked in seeds harboring null alleles of the metal transporters-encoding genes, *AtNRAMP3* and *AtNRAMP4* (Lanquar et al., 2005). The synchrotron-generated x-ray fluorescence of metals (XRF), analyzed by microtomography is, to date, the most powerful technique for multiple metal imaging, although for obvious reasons this technique is not readily accessible to everyone. The analysis of Arabidopsis seeds by XRF tomography has generated crucial information on Fe localization and on the function of the tonoplastic Fe transporter VIT1 (Kim et al., 2006). First, it was shown that in dry seeds, the Fe distribution superimposed the vascular system of the embryo. This pattern is specific for Fe since zinc (Zn) was found uniformly throughout the embryo whereas manganese (Mn) was localized in the abaxial side of the cotyledons. Second, the loss-of-function mutation in *VIT1* disturbed the pattern of Fe distribution, resulting in a diffuse localization in the subepidermal region of the radicle and the cotyledons. These recent discoveries have opened up new questions: Within which precise cell layer(s) is Fe located in the dry seed? What are the new target cells for Fe accumulation in the *vit1-1* mutant? Can we identify the subcellular compartment(s) in which the Fe pools are stored? Can we monitor the kinetics of Fe loading during embryo development and of Fe remobilization during germination? Unfortunately, none of the above-listed techniques of metal imaging can provide together the resolution, the sensitivity, and the simplicity required to address these questions.

Therefore, in this report, we have made use of a powerful method of Fe histochemical staining to establish the loading of Fe during embryo development. The staining, based on a first reaction with ferrocyanide (Perls reagent, reaction I), is further enhanced by reaction with diaminobenzidine (DAB), hydrogen peroxide (H_2O_2), and cobalt (Perls/DAB from now on, reaction II).

$$4Fe^{3+} + 3[Fe^{II}(CN)_6]^{4-} \rightarrow Fe^{III}{}_4[Fe^{II}(CN)_6]_3 \times H_2O \text{ (reaction I)}$$

$$Fe^{III}{}_4\,[Fe^{II}(CN)_6]_3 + \tfrac{1}{2}\,H_2O_2 \rightarrow Fe^{II}{}_4\,[Fe^{II}(CN)_6]_3 + H^+ + O \text{ (reaction II)}$$

This staining procedure, specific for Fe, quick and inexpensive to set up, can be used either on whole Arabidopsis embryos, or, more interestingly, by in situ staining directly on histological sections. With this latter procedure, virtually applicable to any kind of sample, we were able to reach a subcellular resolution. In dry seeds, we have identified that the main pool of Fe is localized in the vacuoles of the endodermal cells. The *vit1-1* mutation provokes the redistribution of Fe in cortex cells of the hypocotyls and in a single subepidermal cell layer in the cotyledons, although Fe is still stored in the vacuoles of these cells. During embryogenesis, Fe is first found in all the cells of both wild-type and *vit1-1* embryos. In the last stages of embryo development, Fe eventually accumulates in the endodermis, a process that is abolished in *vit1-1*.

RESULTS

Fe Detection in the Arabidopsis Embryo Using the Perls Stain Associated to Intensification by DAB/H_2O_2

The Perls method is used to stain in blue Fe deposits in the tissues. Potassium ferrocyanide, the so-called Perls reagent, can react with Fe^{III} to form an insoluble pigment known as Prussian blue. However, Fe concentration in most tissues is low and the threshold of detection using the Perls method is rarely reached. Therefore, staining of Fe can be intensified taking advantage of the redox activity of the Prussian blue. The degradation of H_2O_2 by the Prussian blue, coupled to 3,3′ DAB provokes the formation of a dark-brown coloration due to the polymerization of DAB (Nguyen-Legros et al., 1980). In plants, the Perls stain has already been used to detect Fe in Arabidopsis roots (Green and Rogers, 2004) and embryos (Stacey et al., 2008). These experiments have shown that a Prussian blue precipitate accumulates in the vascular tissues at a high level in mutants overloaded with Fe, but faintly in wild-type plants. We have used the method of intensification of the Perls stain by DAB/H_2O_2, described in animal tissues, to enhance the sensitivity and definition of Fe detection in plants. We first compared the intensity of staining of Arabidopsis embryos obtained by the Perls method alone or by the DAB-enhanced Perls method (Fig. 1A). When the embryos were stained with the Perls reagent, a weak-blue coloration developed around the provascular

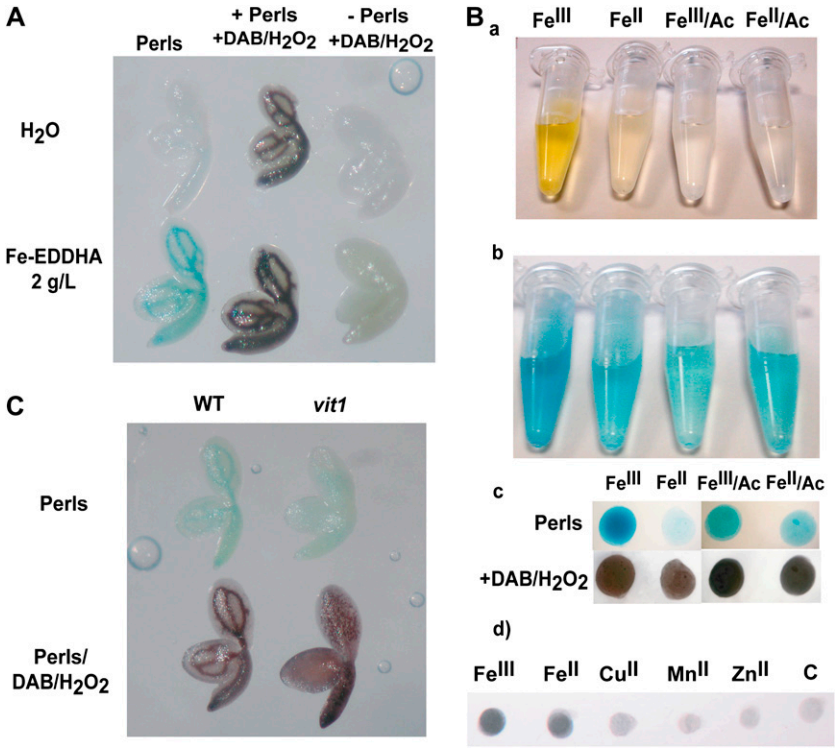

Figure 1. Fe detection in Arabidopsis embryos using the Perls/DAB stain. A, DAB/H_2O_2 intensification is Perls stain dependent. Embryos were dissected from seeds produced by plants irrigated with either water or Fe-ethylenediamine-*N*,*N*′-bis(2-hydroxyphenylacetic acid) (2 g/L) as indicated on the figure. The applied treatment, with or without Perls stain and DAB/H_2O_2 intensification, is indicated in the figure. B, Perls/DAB specificity is not restricted to Fe^{III}. The different Fe solutions used are shown before staining (a), after the Perls reaction (b), dot blotted on nitrocellulose before (c, top lane), and after (c, bottom lane) staining with DAB/H_2O_2; d, Metal specificity test for Perls/DAB stain. C, Effects of mutating *VIT1* on Fe distribution in the embryo. Embryos dissected from wild-type (WT) and *vit1-1* seeds were stained with Perls (top) or Perls/DAB (bottom).

region of the radicle/hypocotyl and the cotyledons (Fig. 1A, Perls column). On the contrary, when Perls-stained embryos were treated with DAB/H_2O_2 (Fig. 1A, +Perls DAB/H_2O_2 column), a strong black precipitate appeared in the region where the Prussian blue had accumulated. As a negative control, when the Perls reagent was omitted in the treatment, no staining was detected in the embryos, showing that the brown staining was strictly Perls dependent and not due to, for example, peroxidase-catalyzed degradation of H_2O_2 inducing the polymerization of DAB (Fig. 1A, −Perls DAB/H_2O_2 column). This result confirms that the sensitivity of the Perls method is drastically enhanced by the DAB/H_2O_2 treatment in plant tissues.

We next tested whether staining by Perls/DAB was quantitative by analyzing embryos produced by plants irrigated with a solution of Fe (Fig. 1A, compare H_2O and Fe-ethylenediamine-*N*,*N*′-bis(2-hydroxyphenylacetic acid) 2 g/L). Using Perls alone, the blue staining was strongly increased in Fe-supplemented embryos, whereas using the Perls/DAB method the black precipitate obtained was strong irrespective of the Fe nutrition of the mother plant. We concluded that although very sensitive, intensification of the Perls staining by DAB/H_2O_2 is less quantitative than Perls staining alone.

It is commonly admitted that the Perls method stains specifically Fe in its ferric form (Fe^{III}) but not in its ferrous form (Fe^{II}). To determine which redox state of Fe could be detected with this technique, we tested in vitro the reactivity of the Perls solution, with or without the DAB/H_2O_2 intensification, with Fe^{II} or Fe^{III} solutions. Perls reacted more strongly with a solution of $FeCl_3$, a source of Fe^{III}, than with a solution of $FeSO_4$, a source of Fe^{II} (Fig. 1B, sections a and b). Moreover, when Fe^{III} was reduced to Fe^{II} with ascorbic acid (FeIII/Ac), the staining intensity decreased, indicating that although the Perls solution reacts preferentially with Fe^{III}, reaction with Fe^{II} is possible (Fig. 1B, section b). To test the reactivity of Perls/DAB with Fe^{II} or Fe^{III}, the Perls reactions (shown in Fig. 1B, section b) were blotted on a nitrocellulose membrane, and the intensification protocol with DAB/H_2O_2 was applied (Fig. 1B, section c). A black precipitate was detected with both Perls-Fe^{II} and Perls-Fe^{III} complexes, indicating that both Perls-Fe complex species could be stained with DAB/H_2O_2.

The specificity of known Fe ligands is often not restricted to this metal ion. This is the case for bathophenanthroline sulfonate, which is used to quantify Fe^{II} but can also chelate Mn^{II} and Cu^{II}, and for calcein, a fluorescent probe used to image Fe^{III} in animal and plant tissues (Breuer et al., 1995; Thomas et al., 1999), but that can also react with Zn and Mn (http://www.anaspec.com/products/product.asp?id=29761). This prompted us to test whether the Perls/DAB method is specific for Fe. To that aim, we have realized Perls/DAB reactions with equal amounts of copper (Cu), Zn, and Mn in vitro. Among these metals, only Cu produced a weak coloration, above the background (Fig. 1B, section d). To test the Perls/DAB specificity in vivo, we compared the pattern of Fe distribution in the embryo obtained by Perls/DAB staining with that determined by x-ray-based imaging in either wild-type or mutant embryos with altered Fe distribution (Kim et al., 2006). Analysis of Arabidopsis dry seeds

through XRF microtomography established that Fe accumulates around the vascular system of the embryo whereas Mn is located in more peripheral layers in the radicle and the cotyledons and Zn is distributed throughout the embryo. Therefore, the staining pattern by Perls/DAB is compatible with Fe but not with Zn or Mn distribution. Furthermore, a loss-of-function mutation in the *VIT1* gene that encodes a vacuolar Fe transporter was shown to profoundly affect Fe localization in the embryo (Kim et al., 2006). Consistent with this observation, treatment of *vit1-1* embryos with Perls/DAB showed a pattern of staining distinct from the vascular pattern observed in wild-type embryos (Fig. 1D). We therefore concluded that Perls/DAB staining is specific to Fe.

Fe Is Accumulated in Specific Cells in the Embryo

A previous analysis of the metal distribution in Arabidopsis seeds, determined by EDX-based transmission electron microscopy, had established that the highest Fe concentration is found in the procambium region of both the hypocotyl-radicle axis and the cotyledons (Lott and West, 2001). To identify the cell types involved in Fe storage in the embryo, cross sections were performed in wild-type, *vit1-1*, and *nramp3 nramp4* embryos stained by the Perls/DAB method (Fig. 2). In wild-type embryos, the staining was concentrated in a single cell layer surrounding the provascular bundle in both the cotyledons and the hypocotyl (Fig. 2, A and B). This localization did not correspond to the procambium. Indeed, activity of the *AtHB8* promoter, a procambial marker, is located in a region distinct from and surrounded by the ring of Fe staining (Fig. 2L). Instead, observations of the sections identify unambiguously the Fe storage layer as the endodermis. This result was further supported by the longitudinal section of the hypocotyl/radicle axis of immature embryos stained with Perls/DAB. Upon periclinal division of the initial endodermis cell, which gives rise to two daughter cells belonging to the endodermis and cortex layers, Fe accumulation was lost in the cortical daughter cell (Fig. 2, J and K), indicating that Fe specifically accumulates in differentiated endodermis cells. In *vit1-1* however, cross section of the embryo revealed a black precipitate in the subepidermal cells of cotyledons and hypocotyl (Fig. 2D). This aberrant localization did not appear to be the consequence of an abnormal development of the endodermis in *vit1-1* embryos, as shown by Schiff counterstaining of the sections (Fig. 2, C and F). Finally, in embryos from the *nramp3 nramp4* mutant the distribution of Fe was identical to wild type (Fig. 2, G and H). This suggested that the double mutation did not affect Fe storage but only Fe remobilization. In conclusion, the microscopic analysis of embryos stained by Perls/DAB identified endodermis, but not procambium, as the main site of Fe accumulation in mature embryos.

Fe Distribution in a Mutant of Root Development

To investigate whether proper formation of the endodermis is required for Fe storage in the embryo,

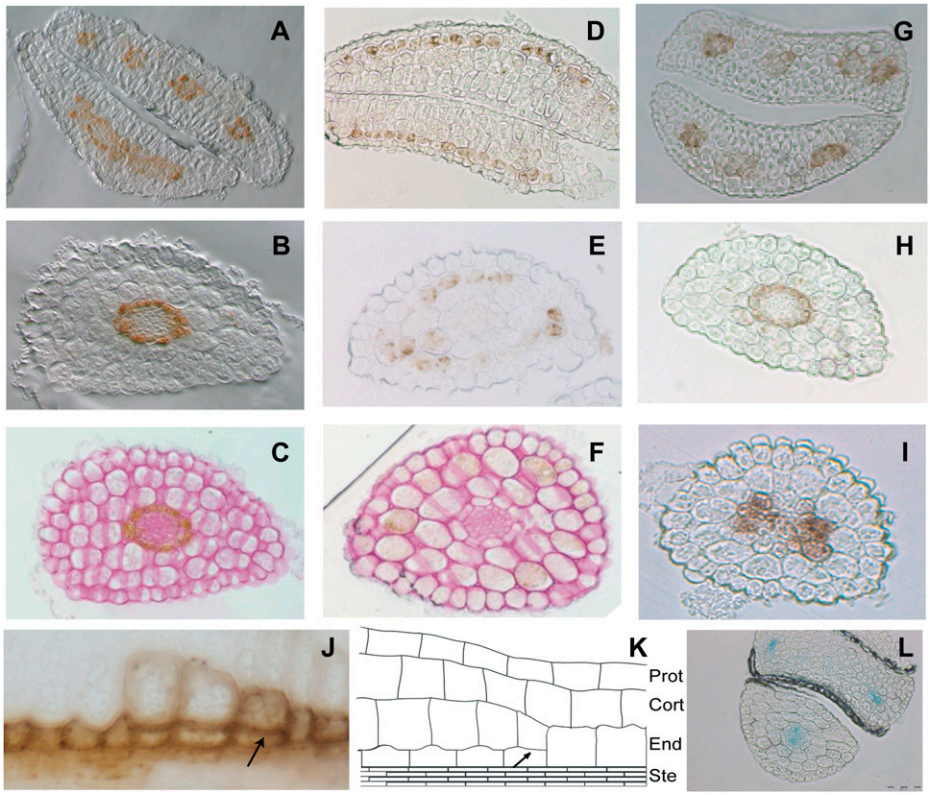

Figure 2. Fe is stored in the endodermis layer in the embryo. Microscopic analysis: Wild-type Col-0 (A–C), *nramp3 nramp4* (g and h), *vit1-1* (D–F), and *shr* (*shr-2*; i) dry seed embryos were dissected, stained with Perls/DAB, embedded in Technovit resin, and cut transversally. A, D, and G, Cotyledons. B, E, H, and I, Hypocotyl. C and F, Hypocotyl section counterstained with the Schiff reagent. J, Longitudinal section across the hypocotyl/radicle axis of a wild-type embryo dissected at the green cotyledons stage and stained with Perls/DAB. K, Endodermal-periclinal division scheme (adapted from Scheres et al., 1995). Prot, Protodermis; Cort, cortex; End, endodermis; Ste, stele. L, Histochemical analysis of GUS activity in dry seed embryos isolated from a p*AtHB8-GUS* transgenic line.

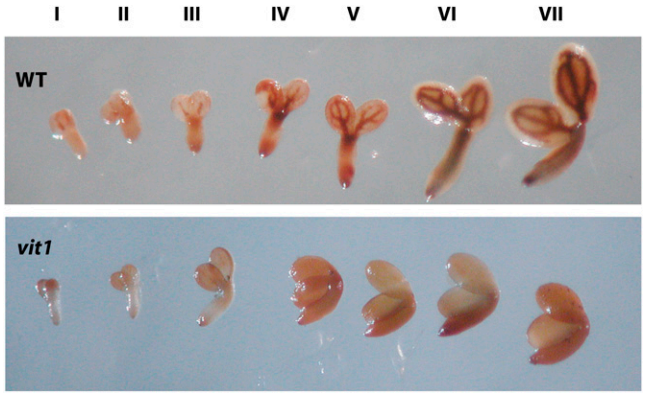

Figure 3. Fe accumulation during embryo development. Wild-type (WT; above) and *vit1-1* (below) embryos dissected from siliques at different maturation stages, from torpedo (I) until mature embryo before desiccation (VII), and stained with Perls/DAB.

we analyzed Fe distribution in *short root* (*shr*), a mutant of root development that lacks endodermis (Scheres et al., 1995). Dry seed embryos of *shr-2* were stained with Perls/DAB, embedded in resin, and sectioned at the level of the hypocotyl/radicle axis. In the absence of endodermis, in the *shr-2* mutant, Fe accumulation was observed in the stele of the hypocotyl and followed a polar distribution (Fig. 2I). We concluded that in the embryo, the endodermis layer, but not the cortex, is essential for proper Fe distribution in the embryo and strongly suggests that, already at this early stage, endodermis forms a barrier that controls Fe access to the stele.

Fe Loading during Embryo Development

To determine the kinetics of Fe accumulation during embryogenesis, Arabidopsis embryos were dissected at different stages of development and stained with Perls/DAB. The embryos presented in Figure 3 are the torpedo (I), walking-stick (II, III), curled cotyledons (IV), and green cotyledons (V, VI, VII) stages. Fe accumulation was already visible at the torpedo stage as a faint line located in the center of the cotyledons where the provascular tissue will differentiate (Fig. 3, top section). At the curled-cotyledon stage, staining of Fe clearly followed the line of the vascular system in the cotyledons and strongly accumulated at the apical meristem of the hypocotyl. At the subsequent stages, Fe accumulation was also observed in the vascular region throughout the hypocotyl-radicle axis (Fig. 3). We then stained *vit1-1* embryos at the same stages and compared to wild-type embryos to determine when, during the development, Fe patterning is altered. Until the walking-stick stage, staining of *vit1-1* embryos was detected weakly in the provascular traces, identical to wild-type embryos. Later on, however, Fe failed to reach the vascular region in *vit1-1*, as in wild-type embryos, but instead remained diffuse (Fig. 3). Thus, Fe patterning in *vit1-1* embryos is affected as soon as its accumulation is detectable in the wild-type plant. Interestingly, *VIT1* mRNA accumulation was found in microarrays analyses to be highest in seeds at the torpedo stage and to decrease thereafter (http://www.bar.utoronto.ca/efp/cgi-bin/efpWeb.cgi). Altogether, these results confirm and strengthen the previously reported involvement of VIT1 in the distribution of embryonic Fe pools.

Vacuole Fe Mobilization during Germination

The importance of the vacuolar Fe pool for seed germination has been underscored in a genetic and physiological study of AtNRAMP3 and AtNRAMP4, two vacuolar metal transporters of Arabidopsis. Interestingly, germination in low Fe nutrition is impaired in a double *nramp3 nramp4* mutant due to a failure to release Fe stored in globoid structures of the vacuole (Lanquar et al., 2005). Consistent with the reported defect of *nramp3 nramp4* seeds to remobilize vacuolar Fe during germination, we observed a stronger Perls/DAB staining in 4-d-old *nramp3 nramp4* seedlings compared to wild type (Fig. 4). Qualitatively, however, the pattern of staining in the vascular area was unchanged in *nramp3 nramp4* seedlings (Fig. 4). From this result, we concluded that the vacuolar Fe pool remobilized by AtNRAMP3 and AtNRAMP4 during germination (Lanquar et al., 2005) and the Fe pool located in the endodermis by the Perls/DAB method (this work) are identical.

In Situ Fe Localization during Embryo Development

To increase the resolution of the method, a modification of the staining procedure presented above has been introduced and consists in the staining of

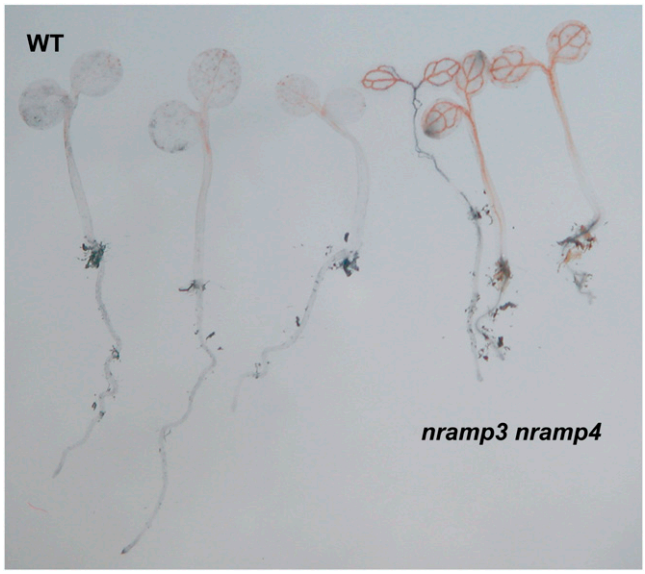

Figure 4. Fe distribution during seed germination. Fe accumulation in young seedlings. Wild-type (WT) and *nramp3 nramp4* seeds were germinated on soil for 4 d, then stained with Perls/DAB.

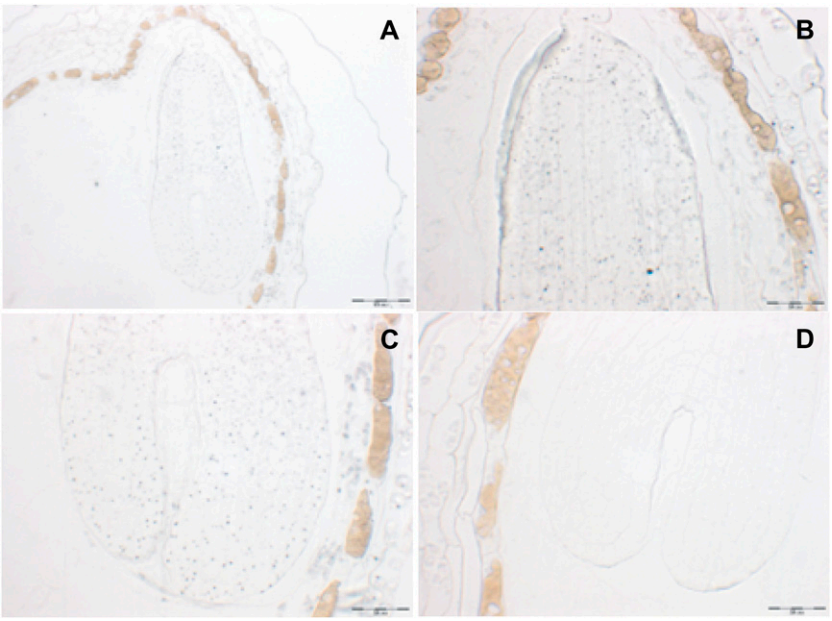

Figure 5. Fe distribution in wild-type embryos at the torpedo stage. Wild-type seeds at the torpedo stage dissected from siliques were embedded in Technovit resin and sectioned (3 μm) at the level of the hypocotyl/radicle axis, then stained with Perls/DAB (A–C) or DAB alone as a negative control of staining (D). A and D, Whole embryos. B, Radicle. C, Cotyledons. The scale bar represents either 50 μm (A) or 20 μm (B and C).

Fe directly on histological sections (termed in situ staining). With this staining protocol, the presence of Fe appeared as small black dots (Figs. 5–8, A–C). The coloration was absent in control samples where Perls staining was omitted (Figs. 5D, 6D, 7E, and 8E). In wild-type embryos taken at the torpedo stage (corresponding to stage I in Fig. 3), Fe was uniformly distributed in all the tissues (Fig. 5, A–C). The staining was rather pale, indicating that the cellular Fe concentration is not very high at that stage. Moreover, the pattern of Fe distribution in wild-type and *vit1-1* mutant was identical (Fig. 6, A–C, to be compared with Fig. 5, A–C).

We then have analyzed Fe distribution in embryos corresponding to stage VI, before desiccation (Figs. 7 and 8). In wild-type embryos, a strong staining was visible in cells surrounding the provascular system (Fig. 7, A–C). Compared to the resolution obtained with sections of previously stained tissues, using the in situ staining procedure enabled visualization of Fe at the subcellular level (compare Fig. 2B and Fig. 7C). In cross sections of the cotyledons (Fig. 7B) and hypocotyl (Fig. 7C) regions, Fe was concentrated in intracellular structures most likely corresponding to vacuoles, based on their shape, size, and on the protein accumulation revealed by staining with naphtol blue black and periodic acid/Schiff (Fig. 7D). In the *vit1-1* mutant, Fe misdistribution was quite remarkable using the in situ staining method (Fig. 8A). In the cotyledons of *vit1-1*, Fe was stored in a single subepi-

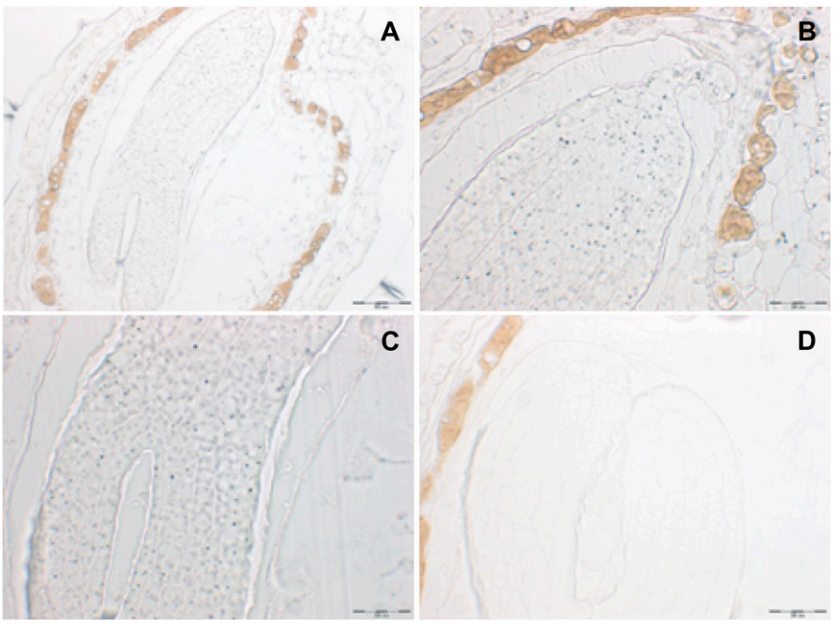

Figure 6. Fe distribution in *vit1-1* embryos at the torpedo stage. *vit1-1* seeds at the torpedo stage dissected from siliques were embedded in Technovit resin and sectioned (3 μm) at the level of the hypocotyl/radicle axis, then stained with Perls/DAB (A–C) or DAB alone as a negative control of staining (D). A and D, Whole embryos. B, Radicle. C, Cotyledons. The scale bar represents either 50 μm (A) or 20 μm (B and C).

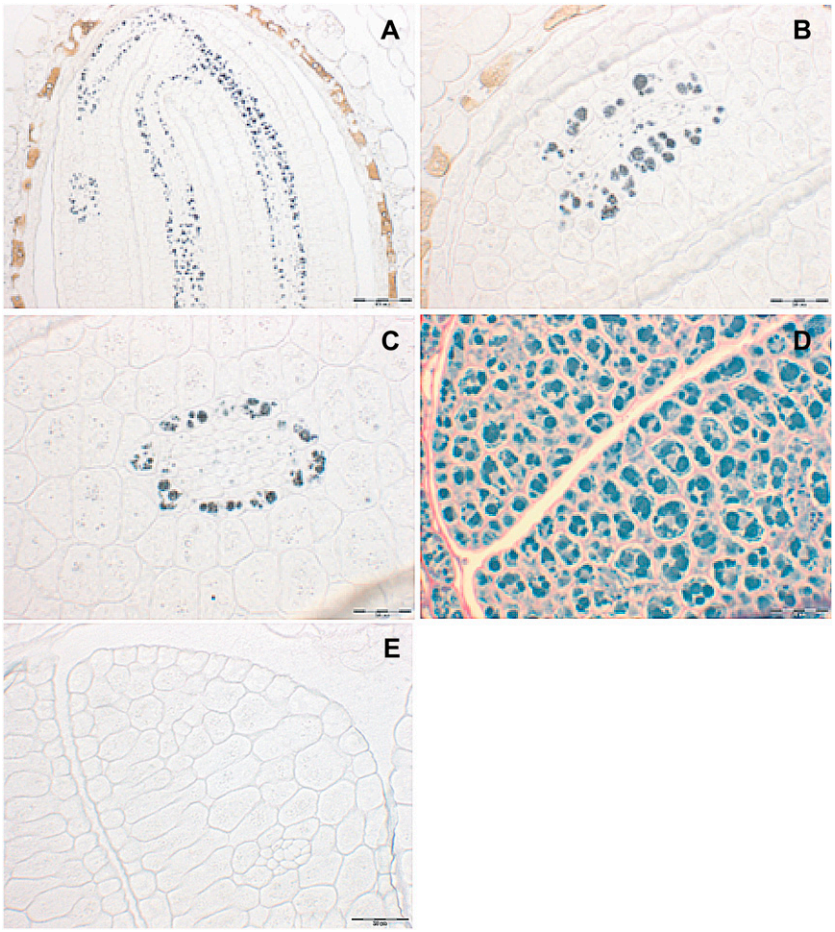

Figure 7. Fe distribution in wild-type embryos at the mature stage. Wild-type seeds at the mature stage, before desiccation, were dissected from siliques, embedded in Technovit resin, and sectioned (3 μm) in the hypocotyl/radicle axis were stained with Perls/DAB (A–C) or DAB alone as a negative control of staining (E). A and E, Whole embryos. B and D, Cotyledons. C, Radicle. D, Periodic acid-Schiff-naphthol blue-black staining. Scale bar represents either 50 μm (A and E) or 20 μm (B–D).

dermal cell layer located in the abaxial side (Fig. 8B). In the hypocotyls/radicle region, Fe was detected in the two layers of cortex cells (Fig. 8C). Despite the difference of tissue distribution between the two genotypes, however, the intracellular staining in *vit1-1* was qualitatively indistinguishable from the intracellular staining in wild-type embryos. We therefore concluded that in the *vit1-1* mutant too, Fe is stored in the vacuoles, albeit in different cell types.

DISCUSSION

The imaging of metals with a subcellular resolution can be considered as a holy grail for the community working in this particular field. Recently, two reports have provided important information on the localization of Fe in Arabidopsis seeds, either by EDX/inelastic scattered electron microscopy on transmission electron micrographs (Lanquar et al., 2005) or by XRF tomography (Kim et al., 2006). In the former it was shown that the principal source of Fe for germination was located in vacuoles whereas the latter showed the role of a vacuolar transporter in the Fe patterning in the dry seed. The aim of this work was to complement these fragmented data on the loading and distribution of Fe in the seed. In this study, we have adapted to plant samples a histochemical staining of Fe, the Perls coloration associated with DAB/H_2O_2 intensification. This procedure, which, to our knowledge, was reported for the first time in 1980 (Nguyen-Legros et al., 1980), has proven to be extremely sensitive. Adaptation of this method to plant tissues, however, has required subtle technical modifications that are now assembled in an easy-to-use protocol available to the plant community. In the first place, our work demonstrates that contrary to Perls staining that detects only Fe^{III}, the Perls/DAB protocol enables to stain both Fe^{II} and Fe^{III} (Fig. 1B). The intensification is based on the oxidative polymerization of DAB by H_2O_2 in the presence of Fe^{III} after reaction with ferrocyanide (Meguro et al., 2007). If both ferrous and ferric ions are present in a sample, two different reactions will occur:

$$Fe^{III}{}_4\,[Fe^{II}(CN)_6]_3 + \tfrac{1}{2}\,H_2O_2 \rightarrow Fe^{II}{}_4\,[Fe^{II}(CN)_6]_3 + H^+ + O$$

$$Fe^{II}{}_4\,[Fe^{II}(CN)_6]_3 + \tfrac{1}{2}\,H_2O_2 \rightarrow Fe^{III}{}_4\,[Fe^{II}(CN)_6]_3 + OH^-$$

Overall, it is clear from these two reactions that the addition of H_2O_2 to Fe that has reacted with Perls,

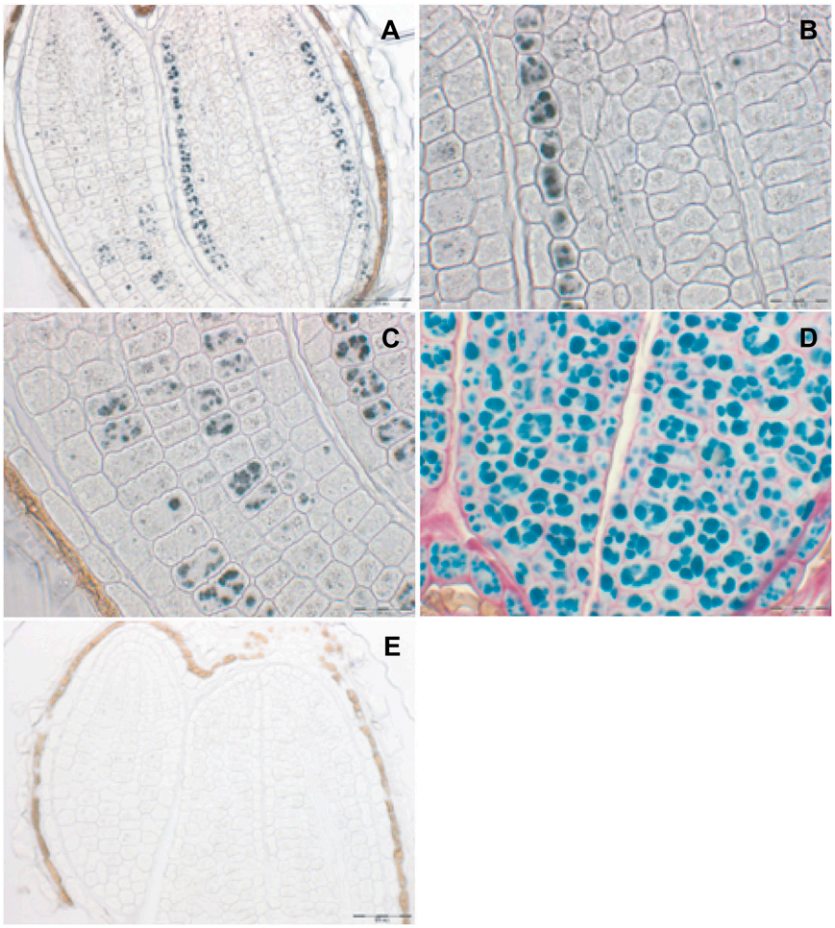

Figure 8. Fe distribution in *vit1-1* mature embryos. *vit1-1* seeds at the mature stage, before desiccation, were dissected from siliques, embedded in Technovit resin, and sectioned (3 μm) in the hypocotyl/radicle axis were stained with Perls/DAB (A–C) or DAB alone as a negative control of staining (E). A and E, Whole embryos. B and D, Cotyledons. C, Radicle. D, Periodic acid-Schiff-naphthol blue-black staining. Scale bar represents either 50 μm (a and e) or 20 μm (b–d).

irrespective of the redox status, will generate a redox cycle between Fe^{III} and Fe^{II}, producing oxygen and thus brown pigments.

Second, we have unambiguously shown that the Perls/DAB method stains specifically Fe. The specificity was established in vitro by testing the reactivity of Perls/DAB with Cu, Zn, and Mn (Fig. 1B, section d). Although a very faint coloration could be obtained with Cu, the very low concentrations of Cu found in vivo, compared to Fe, imply that cross staining is very unlikely to occur. Moreover, the histological staining of Fe in cross sections of wild-type embryos, around the vascular tissues, is indeed Fe specific since the elemental analysis had previously established that Zn was almost evenly distributed in the embryo whereas Mn was highly concentrated in a subepidermal abaxial cell layer of the cotyledons (Kim et al., 2006).

In an earlier report on the elemental composition of globoids in Arabidopsis seeds using EDX electron microscopy, high Fe concentrations were detected in the procambium region (Lott and West, 2001). To our knowledge, this was the first examination of Fe localization at the tissue level in plants, reporting that Fe was located in a procambial region of the embryo, a result that has been accepted as such ever since. We have refined these initial observations with thin sections of embedded stained embryos. In the radicle axis Fe accumulated in a single layer of cells surrounding the procambial sheath forming the provascular system (Fig. 2B). In the *vit1* mutant the loss of patterning was not due to the loss of a particular cell layer since, from an histological point of view, all the typical cell types were maintained in the mutant: one protodermis, two cortex, and one endodermal layers surrounding the provascular cells. We further confirmed the endodermal identity of this cell layer by the analysis of longitudinal sections of embryos. In Arabidopsis, the radial pattern of cell types in the root and hypocotyl is established during embryogenesis. The cortex/endodermis differentiation is the result of successive anticlinal and periclinal divisions of an initial cell of the root meristem (Di Laurenzio et al., 1996). In the transition zone between the root tip and the hypocotyl, a second periclinal division occurs to generate a second layer of cortex, typical of the hypocotyl (Scheres et al., 1995). In longitudinal sections of Perls/DAB-stained embryos, at the root tip-hypocotyl transition zone, we have observed that after the periclinal division, Fe remains in the endodermal cell line whereas its accumulation is lost after two divisions of the newly formed cortex layer (Fig. 2J). Finally our results indicate that the endodermis may act as a physical barrier

for Fe radial movement since (1) Fe is not detectable in the central provascular cells in wild-type embryos, (2) in the *vit1* mutant that contains an endodermis layer, Fe is located in the cortex, and (3) in a *shr* mutant lacking endodermis Fe accumulates in the central cylinder (Fig. 2). It is rather surprising to find exclusion mechanisms very early in the differentiation of tissues. The exclusion of Fe from the provasculature may be related to its potential cytotoxicity, in particular for this cell type that serves as ground tissue for the further differentiation of xylem and phloem.

The Perls/DAB technique has enabled us to show the temporal and spatial distribution of Fe pools during the embryo development. During this process, the loading of Fe seemed to follow two marked steps with a transition at stage IV, for both wild-type and *vit1* genotypes. Fe was first distributed evenly throughout the embryo (stages I–III), then some accumulation was visible in subdomains of shoot and root meristems (stages IV and V) before being restricted to the vascular system (stages VI and VII; Fig. 3). Such a patterning is remarkably reminiscent of the cell-to-cell movement of solutes and proteins in the Arabidopsis embryo. Indeed, several reports have established that until the torpedo stage, all the cells of the embryo are connected symplastically. Further on, some subdomains tend to be isolated from the rest (shoot and root meristems) and finally, in the mature embryo the vascular system is completely disconnected from the surrounding cells (Kim et al., 2005a, 2005b; Stadler et al., 2005). It is conceivable that the patterning of Fe follows the same movements, but so far the molecular identity of genes that may control this process is unknown.

Using the latest development of the Perls/DAB procedure, the in situ staining, we have been able to localize Fe at the subcellular level, a resolution never reached in plants without having recourse to electron microscopy techniques (Figs. 5–8). Surprisingly, in the vacuolar Fe transporter knockout mutant *vit1-1*, Fe was still found concentrated in vacuoles, but away from the endodermal cells. This observation suggests that other vacuolar Fe transport systems are activated in these particular cells to cope with the accumulation of Fe. Such transport systems may be encoded by *VIT1*-related genes or may belong to other families of transporters. It is indeed striking that in the cotyledons of *vit1-1* Fe accumulates precisely in the cell layer where Mn is located. Since VIT1 and NRAMP proteins have been shown to transport Fe and Mn, it is possible that a protein belonging to one of these families is responsible for the vacuolar storage of Fe in this particular situation. In mature wild-type embryos, we have established that the Fe storage pool in seeds is located in the vacuoles of endodermal cells. Moreover, we have shown that this particular Fe pool is the one remobilized during germination, since in the *nramp3 nramp4* mutant seedlings the vascular Fe persisted, in comparison to wild-type seedlings (Fig. 4). Although not demonstrated so far, it is likely that VIT1 is responsible for the vacuolar transport of Fe uptake by the vacuoles of endodermal cells. We propose a model in which a VIT1-mediated Fe influx in the vacuoles of endodermis could generate a symplastic flux of Fe toward these cells. Eventually, the combined action of vacuolar sequestration and individualization from symplastic connections would lead to the vascular pattern observed. Consistent with this scenario, in the absence of VIT1, the creation of such a Fe flux would fail and Fe would accumulate in cortex cells. To cope with this increased Fe accumulation, cortex cells have the capacity to store Fe in vacuoles. The possibility that this tonoplastic transport activity of unknown identity could be controlled by signals originating from cross-talks between endodermal and cortical cells is very attractive but remains to be demonstrated.

In conclusion, we have adapted and improved a histochemical staining to characterize the loading and storage of Fe in Arabidopsis seeds. This procedure, quick, easy, and inexpensive to set up, has proven to be Fe specific, highly resolutive, and virtually applicable to any kind of plant sample since the pitfall of dye accessibility has been overcome by direct, in situ staining on histological sections. In doing so, we have shown that in Arabidopsis embryos Fe is stored in, and remobilized from, vacuoles of specific cells surrounding the provascular system, the endodermal cells. The Perls/DAB technique is a promising tool that will facilitate the search of new mutants impaired in Fe loading in seeds and be the technique of choice to establish an atlas of Fe distribution in the plant, which is a prerequisite to unravel the molecular events that control Fe homeostasis.

MATERIALS AND METHODS

Arabidopsis Lines and Growth Conditions

All the plant genotypes (Columbia-0, Wassilewskija [Ws], *vit1-1*, *nramp3 nramp4*, and *shr-2* mutants, and the *AtHB8::GUS* transgenic line) were grown in the greenhouse. For the post-germination experiments, Ws and *nramp3 nramp4* mutant seeds were stratified 2 d at 4°C in the dark and grown on soil. Roots were harvested from 4-d-old seedlings and washed with distilled water prior to Fe imaging. The plants were irrigated with water except when stated otherwise.

Perls Stain and DAB/H_2O_2 Intensification

The embryos were dissected from seeds previously imbibed in distilled water for 3 h, using a binocular magnifying lens. The isolated embryos were vacuum infiltrated with equal volumes of 4% (v/v) HCl and 4% (w/v) K-ferrocyanide (Perls stain solution) for 15 min and incubated for 30 min at room temperature (Stacey et al., 2008). The DAB intensification method is described in Meguro et al. (2007). After washing with distillated water, the embryos were incubated in a methanol solution containing 0.01 M NaN_3 and 0.3% (v/v) H_2O_2 for 1 h, and then washed with 0.1 M phosphate buffer (pH 7.4). For the intensification reaction the embryos were incubated between 10 to 30 min in a 0.1 M phosphate buffer (pH 7.4) solution containing 0.025% (w/v) DAB (Sigma), 0.005% (v/v) H_2O_2, and 0.005% (w/v) $CoCl_2$ (intensification solution). The reaction was stopped by rinsing with distilled water.

The in vitro assay for Fe^{II} and Fe^{III} was performed as follows: 1 mL of Perls stain solution was mixed with either 2 μL of $FeSO_4$ or $FeCl_3$ at 35 mM and, when necessary, 10 μL of a 57 mM ascorbic acid solution to reduce Fe^{III}. The obtained solutions were dot blotted on a nitrocellulose membrane and further

stained with DAB/H_2O_2 as described earlier for the staining of embryos. For Fe specificity assay of Perls/DAB stain (Fig. 1B, d) 1 mL of Perls stain solution was mixed with either 2 μL of $FeSO_4$, $FeCl_3$, $CuSO_4$, $MnCl_2$, or $ZnCl_2$ at 35 mM, these solution were centrifuged, the supernantant discarded, and 1 mL of intensification solution was added and the tubes were vortexed. Finally, 2 μL were dot blotted on a nitrocellulose membrane.

In Situ Perls/DAB/H_2O_2 Intensification

The isolated embryos were vacuum infiltrated with fixation solution containing 2% (w/v) paraformaldehyde, 1% (v/v) glutaraldehyde, 1% (w/v) caffeine in 100 mM phosphate buffer (pH 7) for 30 min and incubated for 15 h in the same solution. The fixated embryos were washed with 0.1 M phosphate buffer (pH 7.4) three times, and dehydrated in successive baths of 50%, 70%, 90%, 95%, and 100% ethanol, butanol/ethanol 1:1 (v/v), and 100% butanol. Then, the embryos were embedded in the Technovit 7100 resin (Kulzer) according to the manufacturer's instructions and thin sections (3 μm) were made. The sections were deposited on glass slides that were incubated for 45 min in Perls stain solution. The intensification procedure was then applied as described above.

Microscopic Analysis

The embryos stained with Perls/DAB/H_2O_2 were dehydrated in successive baths of 50%, 70%, 90%, 95%, and 100% ethanol, butanol/ethanol 1:1 (v/v), and 100% butanol. Then, the embryos were embedded in the Technovit 7100 resin (Kulzer) according to the manufacturer's instructions and thin sections (7 μm) were made.

Histochemical Localization of GUS Activity

The transgenic Arabidopsis (*Arabidopsis thaliana*) line (Ws ecotype) carrying the chimeric gene p*AtHB8*::*GUS* was kindly provided by Dr. Simona Baima, Unità di nutrizione Sperimentale (Rome). Histochemical GUS staining was performed as described in Elorza et al. (2004) using 1 mM of 5-bromo-4-chloro-3-indolyl-β-D-glucuronide as a substrate (Jefferson et al., 1987). For the microscopic analysis the embryos were dehydrated, embedded in Technovit resin, and microtome sections were obtained as previously described.

Sequence data from this article can be found in the GenBank/EMBL data libraries under accession numbers At2g01770 (*VIT1*), At2g23150 (*AtNRAMP3*), At5g67330 (*AtNRAMP4*), At4g37650 (*shr*), and At4g32880 (*AtHB8*).

ACKNOWLEDGMENTS

We wish to thank Marylou Guerinot for the gift of the *vit1-1* seeds and Niko Geldner for the *shr-2* seeds. We also thank Gregory Vert for helpful discussions.

Received July 8, 2009; accepted August 28, 2009; published September 2, 2009.

LITERATURE CITED

Bienfait HF, van den Briel W, Mesland-Mul NT (1985) Free space iron pools in roots: generation and mobilization. Plant Physiol **78:** 596–600

Breuer W, Epsztejn S, Cabantchik ZI (1995) Iron acquired from transferrin by K562 cells is delivered into a cytoplasmic pool of chelatable iron(II). J Biol Chem **270:** 24209–24215

Curie C, Cassin G, Couch D, Divol F, Higuchi K, Le Jean M, Misson J, Schikora A, Czernic P, Mari S (2009) Metal movement within the plant: contribution of nicotianamine and yellow stripe 1-like transporters. Ann Bot (Lond) **103:** 1–11

Di Laurenzio L, Wysocka-Diller J, Malamy JE, Pysh L, Helariutta Y, Freshour G, Hahn MG, Feldmann KA, Benfey PN (1996) The SCARECROW gene regulates an asymmetric cell division that is essential for generating the radial organization of the Arabidopsis root. Cell **86:** 423–433

Durrett TP, Gassmann W, Rogers EE (2007) The FRD3-mediated efflux of citrate into the root vasculature is necessary for efficient iron translocation. Plant Physiol **144:** 197–205

Eide D, Broderius M, Fett J, Guerinot ML (1996) A novel iron-regulated metal transporter from plants identified by functional expression in yeast. Proc Natl Acad Sci USA **93:** 5624–5628

Elorza A, Leon G, Gomez I, Mouras A, Holuigue L, Araya A, Jordana X (2004) Nuclear SDH2-1 and SDH2-2 genes, encoding the iron-sulfur subunit of mitochondrial complex II in Arabidopsis, have distinct cell-specific expression patterns and promoter activities. Plant Physiol **136:** 4072–4087

Green LS, Rogers EE (2004) FRD3 controls iron localization in Arabidopsis. Plant Physiol **136:** 2523–2531

Jefferson RA, Kavanagh TA, Bevan MW (1987) GUS fusions: beta-glucuronidase as a sensitive and versatile gene fusion marker in higher plants. EMBO J **6:** 3901–3907

Kim I, Cho E, Crawford K, Hempel FD, Zambryski PC (2005a) Cell-to-cell movement of GFP during embryogenesis and early seedling development in Arabidopsis. Proc Natl Acad Sci USA **102:** 2227–2231

Kim I, Kobayashi K, Cho E, Zambryski PC (2005b) Subdomains for transport via plasmodesmata corresponding to the apical-basal axis are established during Arabidopsis embryogenesis. Proc Natl Acad Sci USA **102:** 11945–11950

Kim SA, Punshon T, Lanzirotti A, Li L, Alonso JM, Ecker JR, Kaplan J, Guerinot ML (2006) Localization of iron in Arabidopsis seed requires the vacuolar membrane transporter VIT1. Science **314:** 1295–1298

Lanquar V, Lelievre F, Bolte S, Hames C, Alcon C, Neumann D, Vansuyt G, Curie C, Schroder A, Kramer U, et al (2005) Mobilization of vacuolar iron by AtNRAMP3 and AtNRAMP4 is essential for seed germination on low iron. EMBO J **24:** 4041–4051

Lott JNA, West MM (2001) Elements present in mineral nutrient reserves in dry Arabidopsis thaliana seeds of wild type and pho1, pho2, and man1 mutants. Can J Bot **79:** 1292–1296

Meguro R, Asano Y, Odagiri S, Li C, Iwatsuki H, Shoumura K (2007) Nonheme-iron histochemistry for light and electron microscopy: a historical, theoretical and technical review. Arch Histol Cytol **70:** 1–19

Nguyen-Legros J, Bizot J, Bolesse M, Pulicani JP (1980) "Diaminobenzidine black" as a new histochemical demonstration of exogenous iron (author's transl). Histochemistry **66:** 239–244

Ravet K, Touraine B, Boucherez J, Briat JF, Gaymard F, Cellier F (2009) Ferritins control interaction between iron homeostasis and oxidative stress in Arabidopsis. Plant J **57:** 400–412

Robinson NJ, Procter CM, Connolly EL, Guerinot ML (1999) A ferric-chelate reductase for iron uptake from soils. Nature **397:** 694–697

Scheres B, Dilaurenzio L, Willemsen V, Hauser MT, Janmaat K, Weisbeek P, Benfey PN (1995) Mutations affecting the radial organization of the Arabidopsis root display specific defects throughout the embryonic axis. Development **121:** 53–62

Shikanai T, Muller-Moule P, Munekage Y, Niyogi KK, Pilon M (2003) PAA1, a P-type ATPase of *Arabidopsis*, functions in copper transport in chloroplasts. Plant Cell **15:** 1333–1346

Stacey MG, Patel A, McClain WE, Mathieu M, Remley M, Rogers EE, Gassmann W, Blevins DG, Stacey G (2008) The Arabidopsis AtOPT3 protein functions in metal homeostasis and movement of iron to developing seeds. Plant Physiol **146:** 589–601

Stadler R, Lauterbach C, Sauer N (2005) Cell-to-cell movement of green fluorescent protein reveals post-phloem transport in the outer integument and identifies symplastic domains in Arabidopsis seeds and embryos. Plant Physiol **139:** 701–712

Strasser O, Kohl K, Romheld V (1999) Overestimation of apoplastic Fe in roots of soil grown plants. Plant Soil **210:** 179–187

Thomas F, Serratrice G, Beguin C, Aman ES, Pierre JL, Fontecave M, Laulhere JP (1999) Calcein as a fluorescent probe for ferric iron: application to iron nutrition in plant cells. J Biol Chem **274:** 13375–13383

Vert G, Grotz N, Dedaldechamp F, Gaymard F, Guerinot ML, Briat JF, Curie C (2002) IRT1, an *Arabidopsis* transporter essential for iron uptake from the soil and for plant growth. Plant Cell **14:** 1223–1233